Cement and Concrete Research 39 (2009) 833–842

Contents lists available at ScienceDirect

Cement and Concrete Research

journal homepage: http://ees.elsevier.com/CEMCON/default.asp

Phase development in conventional and active belite cement pastes by Rietveld analysis and chemical constraints

Antonio J.M. Cuberos [a], Ángeles G. De la Torre [a], M. Carmen Martín-Sedeño [a], Laureano Moreno-Real [a], Marco Merlini [b], Luis M. Ordónez [c], Miguel. A.G. Aranda [a,*]

[a] Departamento de Química Inorgánica, Universidad de Málaga, 29071 Málaga, Spain
[b] European Synchrotron Radiation Facility, ESRF, BP220 F-38043 Grenoble, France
[c] Unidad Técnica de Investigación de Materiales, AIDICO, Avda. Benjamín Franklin, 17 Paterna, Valencia, Spain

ARTICLE INFO

Article history:
Received 11 January 2009
Accepted 11 June 2009

Keywords:
Alkali activated cement
Hydration products
X-ray diffraction
Quantitative phase analysis

ABSTRACT

High belite cements may be an alternative to reduce CO_2 emissions. Although CO_2 emissions may be depleted up to 10%, unfortunately, the hydration reactivity of belite phases is slow which leads to low mechanical strengths at early ages. In order to enhance their hydraulic reactivity, the activation of these cements by doping with alkaline oxides has been proposed. Here, we have synthesised a laboratory belite clinker without activation (47 wt.% of β-C_2S and 19 wt.% of α_H'-C_2S) and two alkaline oxide activated clinkers (one with 13 wt.% of β-C_2S, 24 wt.% of α_H'-C_2S and 19 wt.% of α-C_2S; and the second with 12 wt.% of β-C_2S, 42 wt.% of α_H'-C_2S and 5 wt.% of α-C_2S). We have also developed a methodology to analyse quantitatively the phase evolution of cement pastes and we have applied it to these high belite cements. Rietveld quantitative phase analysis of synchrotron X-ray powder diffraction data, together with chemical constraints, is used to determine the phase development up to 1 year of hydration in the belite cement pastes. β-C_2S almost does not react during the first 3 months, meanwhile α_H'-C_2S reacts on average more than 50% in the same period. Moreover, the degree of reaction of α-C_2S is slightly larger (on average about 70% after three months) than that of α_H'-C_2S. Full phase analyses are reported and discussed including the time evolution of amorphous phases and free water.

1. Introduction

High belite cements (HBCs) were proposed as an alternative to deplete CO_2 emissions in the cement production process [1–4]. Cement nomenclature will be used hereafter, i.e. C = CaO, S = SiO_2, A = Al_2O_3, F = Fe_2O_3, $\bar{S}$ = SO_3, $\bar{C}$ = CO_2 and H = H_2O. These cements contain more than 50 wt.% of C_2S, also named belite. HBCs need less calcium than ordinary Portland cements (OPCs), releasing ~0.50 tons of CO_2 per ton of clinker, instead of 0.54 tons of CO_2. Furthermore, the optimum clinkerization temperature for HBCs production is roughly 100 ºC lower than that for OPCs, which also reduce CO_2 emissions from fuel burning [5]. However, HBCs are more difficult to mill and, chiefly, their slow reactivity leads to low mechanical strengths at early ages. In order to overcome these drawbacks, activation of these materials is highly desirable [6–9]. Most of these attempts to enhance HBCs hydraulic reactivity have concerned the stabilization of high-temperature polymorphs of C_2S (i.e. α forms) at room temperature which are more reactive [10–12]. Recently, the clinkerization process of these materials and the role of minor elements were investigated *in-situ* by SXRPD [13].

On the other hand, X-ray powder diffraction (XRPD) is the appropriate technique to identify and quantify the crystalline phase(s) in mixtures. Applied research in this field has sky-rocketed by applying the Rietveld methodology [14] to XRPD data in order to obtain quantitative phase analyses (QPA). Examples of these research is the QPA of anhydrous cement materials [15–18], including the quantification of the amorphous fraction by adding a suitable standard [19,20]. A step forward is the quantification of the hydration processes of cements using XRPD and the Rietveld method [21]. However, cement hydration process is very complex and the application of Rietveld methodology is not straightforward. Anhydrous cement may contain more than five crystalline components [22], i.e. Ca_3SiO_5 or C_3S, Ca_2SiO_4 or C_2S,

Table 1
Nominal dosages of clinkers, expressed as oxide, in weigh percent.

	CaO	SiO_2	Al_2O_3	Fe_2O_3	K_2O	Na_2O	MgO	TiO_2	SrO	SO_3	P_2O_5
B_ref	62.81	25.00	6.34	5.23	0.27	0.13	0.07	0.01	0.09	0.01	0.04
B_1.5Na	61.97	24.65	6.25	5.15	0.26	1.50	0.07	0.01	0.09	0.01	0.04
B_1S1NK	61.44	24.19	6.13	5.05	1.01	1.00	0.06	0.01	0.08	1.00	0.03

* Corresponding author. Tel.: +34 952131874; fax: +34 952132000.
E-mail address: g_aranda@uma.es (M.A.G. Aranda).

0008-8846/$ – see front matter © 2009 Elsevier Ltd. All rights reserved.
doi:10.1016/j.cemconres.2009.06.017

$Ca_4Al_2Fe_2O_{10}$ or C_4AF, $Ca_3Al_2O_6$ or C_3A and gypsum ($CaSO_4 \cdot 2H_2O$ or $C\bar{S}H_2$). Anhydrous cements may also contain a non-negligible amorphous fraction depending on the cement type [20,23]. During the first hours of hydration, aluminates will react with sulphate carriers, for instance, C_3A with gypsum. Ettringite [$Ca_3Al(OH)_6 \cdot 12H_2O]_2(SO_4)_3 \cdot 2(H_2O)$ or $C_6A\bar{S}_3H_{32}$] (aka Aft) is formed from this first reaction. Silicate phases also react with water to give an amorphous phase (C–S–H gel) and crystalline $Ca(OH)_2$ (or CH or Portlandite). However, C_3S reacts with water much more rapidly than C_2S does [22,24]. Depending on the mineralogical composition of the cement, other chemical reactions take

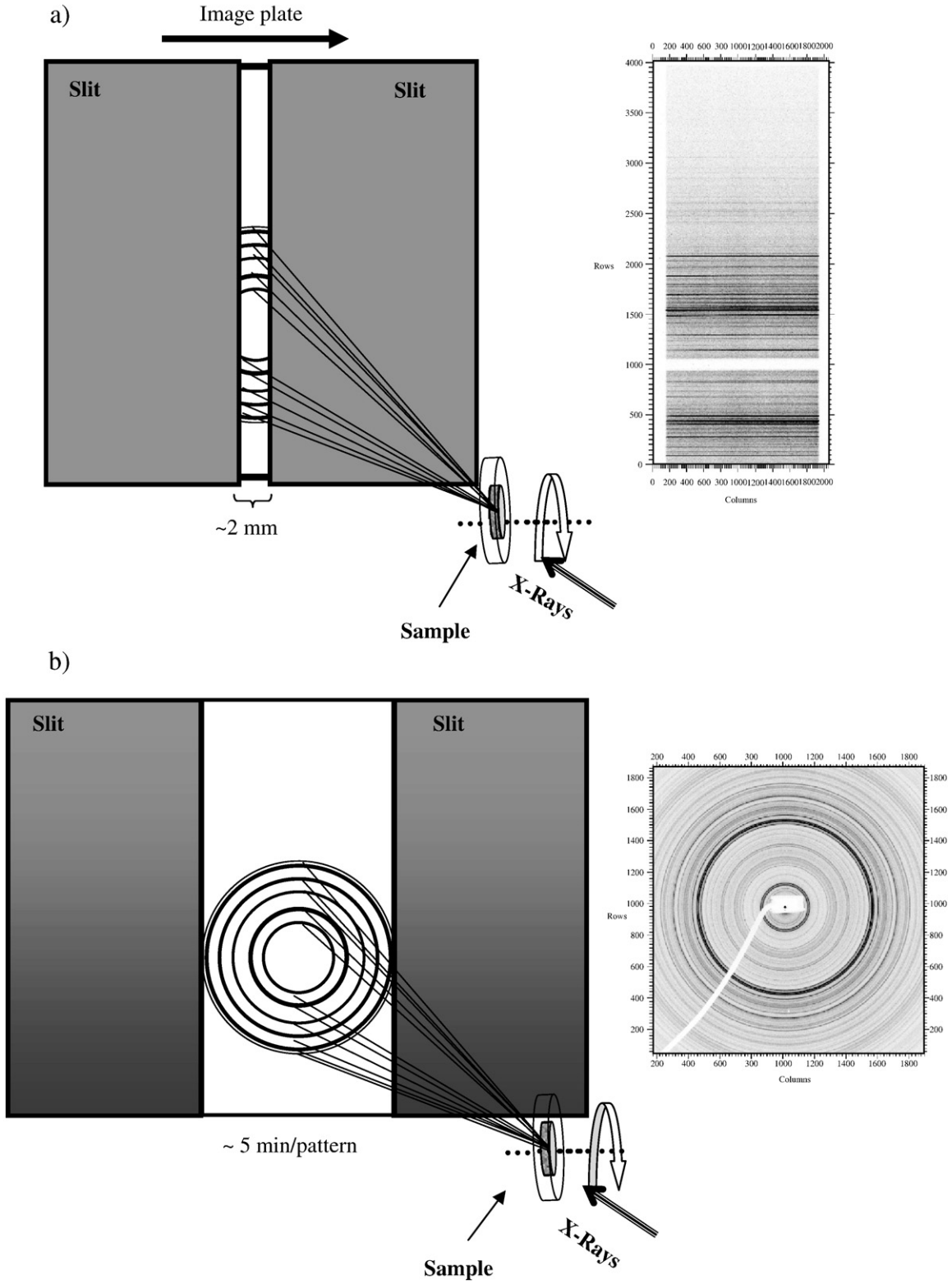

Fig. 1. Illustrations of the SXRPD experimental setups. a) Translating mode and b) 2D full pattern. On the right, the scanned images recorded at the image plate detector.

place. From a chemical point of view, the amount and chemical nature of hydration products (crystalline and amorphous) and the amount of free water will determine final performances of the cement paste. Thus, great efforts have been made to develop analytical tools to quantify these processes. Rietveld analysis results are given as the sum of the phases present normalized to 100% of the crystalline fraction. Therefore, the structural description of all the phases present must be known to perform accurate quantitative phase analysis using Rietveld methodology. If amorphous or non-published structural description or un-known phases are present, this methodology needs the combination of other strategies. An internal standard is usually added prior to hydration in order to quantify the amorphous phases appearing in the process [21,25].

A second step forward in the Rietveld QPA of hydration of cement pastes is the use of chemical constraints. This methodology is used in order to normalize the phase analysis taking into account water bound to crystalline phases, amorphous fractions and free water [26,27]. Furthermore, hydration process is time dependent so the use of synchrotron radiation is very valuable. The initial works were energy-dispersive [28] but these studies have low *d*-spacing resolution (meanwhile, high *d*-spacing resolution is needed for analysing quantitatively complex mixtures). However, the new detectors, i.e. area detectors, let to perform *in-situ* diffraction experiments with very good angular and time-resolutions [29,30]. Therefore, the third step forward is being the use of constant-wavelength *in-situ* synchrotron XRPD (SXRPD) working on transmission geometry which overcomes most of the drawbacks of both laboratory X-ray diffraction and neutron diffraction. Highly energetic synchrotron X-rays allow to analyse a *bulk* sample enhancing particle statistics even on a short time scale. Conversely, neutron studies have low *d*-spacing resolution and require the use of D_2O to reduce incoherent scattering, the effect of D_2O on cement hydration chemistry being known to be significant [31].

The main aim of this work is to study *in-situ* the hydration of active belite cement pastes by Rietveld methodology using constant-wavelength SXRPD data and chemical constraints. The main outcomes are the characterization of the different hydration behaviour of the stabilized C_2S polymorphs. Finally, the different hydration reactions are reported and correlated with calorimetric data.

2. Experimental section

2.1. Synthesis of belite clinkers

Clinkers preparation methodology has been previously reported [8,9]. Table 1 gives the nominal dosages expressed as oxides, and nominal mineralogical compositions, of the three compositions selected to perform this study. One clinker is used as a reference material as it is not activated, hereafter B_ref. The other two clinkers, B_1.5Na and B_1S1NK contain different amounts of activators, i.e. Na_2O and/or K_2O and/or SO_3, indicated in bold in Table 1. The final elemental composition and phase assemblage of these clinkers were previously reported [8,9].

2.2. Preparation of high belite cements

Pure gypsum was added to clinkers to obtain cements. The amount of gypsum was determined by the methodology reported in reference [32]. This author made a study about the optimum amount of gypsum to be added to make cement as a function of alkaline oxides, and reported the following equation:

$$SO_3 = 0.093 \times C_3A + 1.7105 \times Na_2O + 0.9406 \times K_2O + 1.228$$

Where SO_3, Na_2O, K_2O stand for weight percentages of these elements expressed as oxides and C_3A stands for weight percentage of this phase calculated with Bogue equations [33]. Hence, 5.5 wt.% was added to B_ref and 9.4 wt.% to B_1.5Na and B_1S1NK. The cements were milled to have similar Blaine fineness parameters 4160, 4450 and 4320 cm^2/g, respectively. Hereafter, the cements will be named CB_ref, CB_1.5Na and CB_1S1NK.

2.3. In-situ synchrotron X-ray powder diffraction hydration data collection

In-situ SXRPD hydration study was performed in BM08 (GILDA) beamline at the European Synchrotron Radiation Facility, (ESRF, Grenoble, France). Diffraction data were collected with a parallel beam in Debye–Scherrer geometry (transmission) by using a wavelength of 0.68888 Å, determined using FIT2D [34] and the NBS-640b Si standard, $a = 5.43094(4)$ Å. An image plate (IP) detector [35] was used working in two configurations: i) translating mode collecting a small section of the 2D pattern; and ii) 2D full pattern. The translating image plate mode is carried out in order to follow up to 4 h of hydration with good time resolution. The IP moves behind two slits with a constant speed and the diffraction pattern is recorded as a function of time, see Fig. 1a. The slits select a vertical slice of the diffraction rings. The translation speed and the slit size can be chosen to fit the experimental (resolution) requirements. The distance from IP to the sample was 217.0 mm. CB_ref and CB_1.5Na have been measured during the first 4 h using this strategy. The second mode, 2D full pattern, was used for later ages (i.e. more than 4 h), where the slits are removed yielding whole diffraction rings in 5 min, see Fig. 1b. Several patterns at different hydration ages were obtained for the three cements. The images recorded (in both configurations) in the IP detector were recovered using a Fuji BAS2500 laser scanner (16 bit/pixel with a minimum pixel size of 50×50 μm). The SXRPD patterns obtained in translating mode were extracted in 5 min slices using original software available at BM08. 49 patterns were obtained for CB_ref and CB_1.5Na. Powder patterns from 2D images were obtained by integration of the IP using FIT2D software [34].

Pastes were prepared *ex-situ* by mixing the cements with water with a w/c ratio of 0.5. Pastes were immediately loaded in a cylindrical polycarbonate sample holder (15.0 mm diameter × 1.2 mm height) and covered with Kapton slices on both sides. The sample holder was gently spun during data collection, see Fig. 1, to improve the particle statistics and hence to obtain good QPA. The temperature within the experimental hutch was 20 ± 2 ºC.

2.4. Rietveld quantitative phase analysis, RQPA

SXRPD patterns were analyzed by the Rietveld method with X'Pert Highscore Plus software (PANalytical B.V., version 2.2c). Peak shapes were fitted by using the Voigt function [36]. This methodology requires the structural descriptions for all crystalline phases. Table 2 gives the

Table 2
Final phase assemblage for the prepared clinkers and bibliographic information and ICSD collection codes for all crystalline phases.

	CB_ref/ wt.%	CB_1.5Na/ wt.%	CB_1S1NK/ wt.%	Bibliog. ref.	ICSD code
α-C_2S	–	18.7(2)	4.8(1)	[37]	81099
α′$_H$-C_2S	18.5(2)	23.7(3)	41.7(2)	[37]	81097
β-C_2S	46.7(1)	13.0(1)	11.9(3)	[37]	81096
C_3S	13.2(2)	22.4(1)	17.6(1)	[38]	94742
C_3A	10.4(1)	13.0(2)	13.3(1)	[39]	1841
C_4AF	11.5(1)	9.2(1)	10.7(1)	[40]	9197
CSH_2				[41]	151692
AFt				[42]	155395
CH				[43]	15471
AFm-type				[44]	100138
C_2AH_8				See text	–
Tobermorite				[45]	152489
$C\bar{C}$				[46]	157997

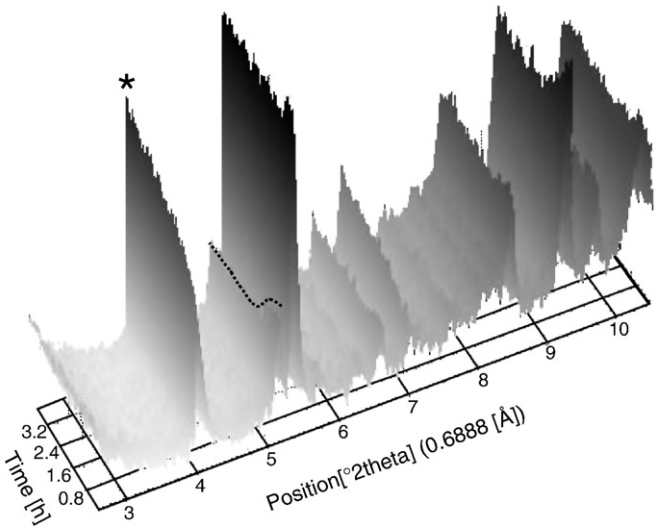

Fig. 2. Low angle region of the time-resolved SXRPD data for belite cement hydration during the first 4 h. The intensity of ettringite main diffraction peak (labeled with *) increases with time, meanwhile the intensity of the main peak of gypsum (highlighted with a dashed line) decreases.

references and ICSD collection codes for all structural descriptions used in this study. Backgrounds were manually established using the base point tool of the software. The refined overall parameters were: cell parameters, zero-shift error, *W* (Gaussian contribution) peak shape parameter and phase fractions. *W* value for β-C_2S, α_H' -C_2S and α-C_2S were constraint to be the same. The atomic parameters (positions, thermal factors and occupation factors) were not refined.

2.5. Isothermal calorimetric study

The isothermal calorimetric study was performed in an eight channel Thermal Activity Monitor (TAM) instrument using glass ampoules. Pastes were prepared with a w/c ratio of 0.5, and the heat flow was collected up to 144 h at 20 ºC.

3. Results and discussion

3.1. Rietveld quantitative phase analysis using SXRPD data

Fig. 2 shows time-resolved SXRPD patterns for CB_ref collected on translating mode during the first 4 h (49 patterns × 5 min/pattern). Belite-cement hydration kinetic is slow, thus, small changes are observed at very early ages and phase assemblage is almost constant during the first 4 h of hydration. Thus, only selected Rietveld QPA results for the first 4 h of hydration are shown in Tables 3 and 4. The remaining QPA results shown in Tables 3–5 have been obtained from 2D full patterns. Quantitative phase analyses were performed using the structural descriptions given in Table 2. However, these results need to be normalized as amorphous phases are appearing, and furthermore, free water is bounding to crystalline and amorphous phases. For instance, these reactions cause β-C_2S fraction to increase 'apparently' during hydration, see Tables 3–5, as the full phase

Table 3
Direct Rietveld QPA results for the hydration of CB_ref cement paste.

	t_0	$t_{0.3}$	t_1	$t_{1.5}$	$t_{2.3}$	t_{17}	t_{23}	t_{43}	t_{67}	t_{90}	t_{114}	t_{2300}	t_{8760}
	0 h	0.3 h	1 h	1.5 h	2.3 h	17 h	23 h	43 h	67 h	90 h	114 h	2300 h	8760 h
β-C_2S	44.1(1)	47.5(5)	47.4(5)	47.0(5)	47.2(5)	48.6(4)	48.5(5)	49.3(5)	52.7(5)	54.9(5)	55.2(5)	57.5(5)	49.5(4)
α_H'-C_2S	17.5(2)	12.1(4)	12.0(4)	12.2(4)	11.9(4)	13.3(4)	14.2(4)	13.5(4)	11.2(4)	10.3(4)	11.2(4)	11.5(4)	9.5(4)
α-C_2S	–	–	–	–	–	–	–	–	–	–	–	–	–
C_3S	12.5(2)	14.9(3)	14.7(3)	14.8(3)	14.7(3)	8.1(3)	7.6(3)	7.0(4)	4.5(3)	3.8(3)	–	–	–
C_3A	9.5(1)	7.1(3)	6.9(3)	7.3(3)	7.0(3)	–	–	–	–	–	–	–	–
C_4AF	10.9(1)	10.7(2)	10.6(2)	10.5(2)	10.4(2)	10.4(2)	9.3(2)	8.6(2)	8.0(2)	8.0(2)	8.1(2)	7.8(2)	8.5(2)
$C\bar{S}H_2$	5.5(–)	4.6(2)	4.1(2)	3.5(2)	3.6(2)	–	–	–	–	–	–	–	–
AFt	–	3.1(2)	4.3(2)	4.7(2)	5.3(2)	10.9(3)	11.2(3)	10.0(3)	9.6(3)	8.8(3)	8.6(3)	7.1(3)	7.3(4)
CH	–	–	–	–	–	3.4(1)	3.3(1)	4.4(1)	5.1(2)	4.6(1)	4.8(2)	5.4(2)	1.5(1)
AFm-12	–	–	–	–	–	0.7(1)	0.8(1)	0.7(1)	0.9(1)	3.0(2)	4.7(2)	4.4(2)	2.7(2)
AFm-14	–	–	–	–	–	3.1(2)	3.2(2)	3.9(2)	4.6(2)	3.6(2)	–	–	–
AFm-ss	–	–	–	–	–	0.9(1)	1.2(1)	1.9(1)	2.5(2)	3.0(2)	3.5(2)	2.8(2)	1.2(1)
C_2AH_8	–	–	–	–	–	0.7(1)	0.7(1)	0.7(1)	0.8(1)	–	–	–	–
Tobermorite	–	–	–	–	–	–	–	–	–	–	3.8(2)	3.6(3)	4.5(1)
AH_3	–	–		–	–	–	–	–	–	–	–	–	0.8(2)
$C\bar{C}$	–	–	–	–	–	–	–	–	–	–	–	–	14.5(3)

Table 4
Direct Rietveld QPA results for the hydration of CB_1.5Na cement paste.

	t_0	$t_{0.3}$	t_1	t_2	t_4	t_{25}	t_{36}	t_{60}	t_{83}	t_{107}	t_{2300}	t_{8760}
	0.0 h	0.3 h	1 h	2 h	4 h	25 h	36 h	60 h	83 h	107 h	2300 h	8760 h
β-C_2S	11.8(1)	13.8(5)	13.9(5)	15.2(5)	15.8(5)	18.3(5)	18.2(5)	18.7(5)	21.2(5)	20.8(5)	23.4(6)	15.1(7)
α_H'-C_2S	21.5(3)	24.4(6)	24.1(6)	24.2(5)	23.7(5)	20.6(5)	19.6(5)	19.4(5)	18.3(6)	18.0(5)	21.6(7)	17.4(7)
α-C_2S	16.9(2)	14.1(4)	13.5(4)	13.3(4)	13.6(4)	10.3(3)	9.2(3)	7.9(3)	8.3(3)	7.8(3)	11.1(4)	14.5(6)
C_3S	20.3(1)	16.6(4)	16.7(4)	16.3(3)	16.1(3)	5.3(3)	3.5(3)	2.3(3)	2.5(3)	2.7(3)	–	–
C_3A	11.9(2)	11.2(5)	11.4(5)	9.3(3)	8.9(3)	4.5(3)	5.0(2)	3.3(2)	3.0(3)	2.8(2)	–	–
C_4AF	8.3(1)	7.0(3)	7.1(3)	7.5(2)	7.7(2)	6.6(2)	5.5(2)	4.7(2)	5.2(2)	5.3(2)	5.6(2)	3.8(3)
$C\bar{S}H_2$	9.4(–)	8.3(2)	7.5(2)	7.4(2)	7.1(2)	–	–	–	–	–	–	–
AFt	–	4.6(2)	5.9(2)	6.8(2)	7.1(2)	27.7(3)	26.4(3)	25.2(3)	23.2(4)	23.9(3)	17.9(4)	21.2(6)
CH	–	–	–	–	–	3.3(1)	3.8(1)	6.4(2)	6.7(2)	6.0(1)	7.6(2)	9.2(3)
AFm-12	–	–	–	–	–	0.4(1)	1.4(1)	1.1(2)	1.0(2)	3.9(2)	6.5(2)	11.3(4)
AFm-ss	–	–	–	–	–	2.9(2)	3.9(2)	5.7(2)	5.6(2)	5.4(2)	–	2.4(1)
Tobermorite	–	–	–	–	–	–	3.4(3)	5.3(3)	5.3(4)	3.4(3)	6.2(4)	3.2(1)
$C\bar{C}$	–	–	–	–	–	–	–	–	–	–	–	1.9(3)

Table 5
Direct Rietveld QPA results for the hydration of CB_1S1NK cement paste.

	t_0	t_2	t_6	t_{30}	t_{40}	t_{64}	t_{87}	t_{2300}	t_{8760}
	0 h	2 h	6 h	30 h	40 h	64 h	87 h	2300 h	8760 h
β-C_2S	10.8 (3)	16.5 (4)	16.4 (4)	22.2 (5)	23.3 (5)	23.2 (5)	23.9 (5)	27.1 (5)	21.0 (8)
α_H'-C_2S	37.8 (2)	40.7 (5)	41.1 (5)	31.8 (5)	30.6 (6)	28.9 (5)	27.4 (5)	29.2 (5)	31.4 (7)
α-C_2S	4.3 (1)	–	–	–	–	–	–	–	–
C_3S	15.9 (1)	16.0 (3)	13.0 (3)	4.5 (3)	3.9 (3)	4.5 (3)	3.2 (3)	–	–
C_3A	12.0 (1)	4.3 (2)	4.2 (2)	1.8 (2)	1.3 (2)	0.8 (2)	–	–	–
C_4AF	9.7 (1)	7.2 (2)	8.1 (2)	5.3 (2)	5.0 (2)	4.4 (2)	5.2 (2)	5.5(2)	3.8(3)
$C\bar{S}H_2$	9.4 (–)	5.8 (2)	3.7 (1)	–	–	–	–	–	–
AFt	–	9.5 (2)	13.5 (2)	26.3 (3)	26.3 (4)	25.8 (4)	23.4 (4)	16.6 (3)	21.3 (6)
CH	–	–	–	3.7 (1)	4.2 (2)	5.1 (2)	4.3 (2)	5.0(1)	7.0(3)
AFm-12	–	–	–	–	–	1.2 (2)	2.8 (2)	7.3(2)	5.7(4)
AFm-14	–	–	–	–	–	–	–	–	–
AFm-ss	–	–	–	4.4 (2)	5.4 (2)	6.1 (2)	5.8 (2)	2.4(1)	3.4(4)
Tobermorite	–	–	–	–		–	4.0 (3)	6.9(3)	5.1(1)
$C\bar{C}$	–	–	–	–	–	–	–		1.2(1)

assemblage is normalized to 100 wt.% of crystalline phases. This raw number make no crystallochemical sense because silicates should decrease (or at least keep constant) as hydration progresses.

The aim of the normalization is to estimate the increase of amorphous phases and the decrease of free water. In the absence of an "unreactive" internal standard, which complicates the analyses, we have adopted a methodology which assumes that β-C_2S is constant (due to its low reactivity with water at early ages). However, after one year of hydration the direct RQPA results indicated that β-C_2S has started to react. Therefore, another phase has to be selected for the renormalization procedure. The inspection of results given in Tables 3–5 yields the following phases as the suitable candidates for renormalization: C_4AF for CB_ref, α-C_2S for CB_1.5Na and α_H'-C_2S for CB_1S1NK; because the phase percentages are increasing from 3 months to one year. We have also assumed that the amount of amorphous phase in the starting cement is negligible. Under these two assumptions, direct Rietveld results may be used to infer the amount of a given phase that is reacting. Once the percentage of a reacting phase is obtained, the stoichiometric reactions are considered.

3.2. Normalization of Rietveld QPA

The initial ($t = 0.0$ h) phase assemblage of each cement paste is 66.7 wt.% of anhydrous cement and 33.3 wt.% of free water (w/c = 0.5). Figs. 3, 4 and 5 show the normalized Rietveld results for the three studied cements. These graphs are divided in two sections for the sake of clarity, (a) reactions of non-silicate phases and (b) reactions where silicates are involved. Solid symbols stand for phases of anhydrous cement, open symbols are products of the hydration process and half-solid symbols are amorphous materials and free water. To perform the normalization, two set of data are considered in each step: normalized phase assemblage at t_x (including free water and amorphous phases) and direct Rietveld phase assemblage at t_y, were x and y stands for hours

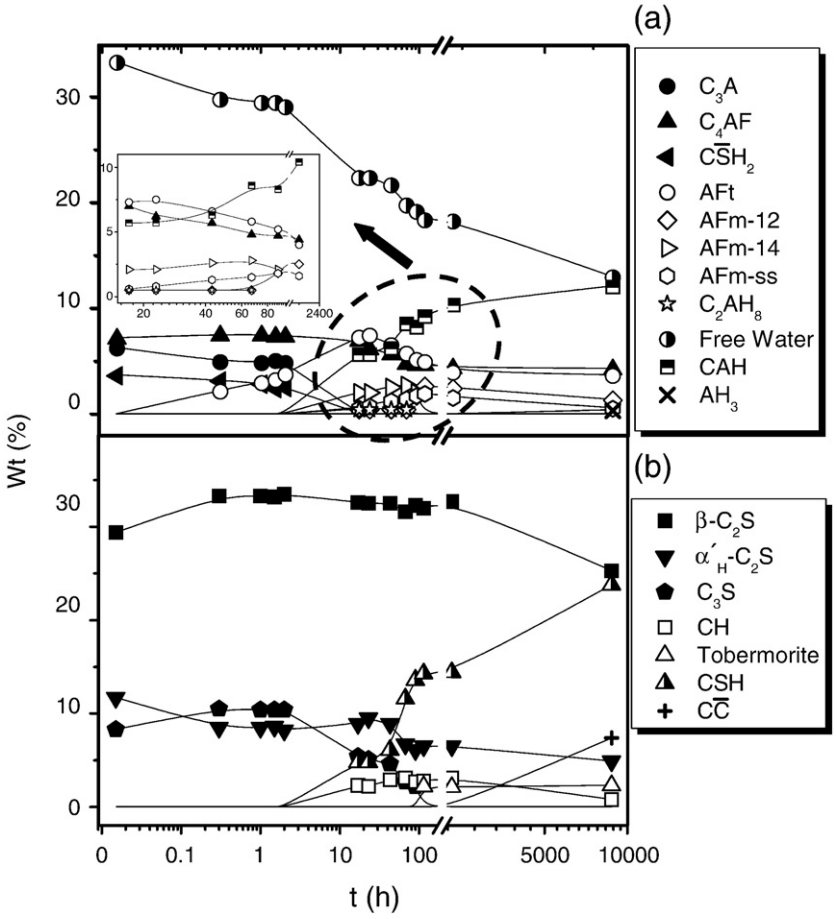

Fig. 3. Normalized quantitative Rietveld results for hydrated CB_ref up to 8760 h, i.e. one year. (a) non-silicate type phases reactions and (b) silicate reactions. The drop of Portlandite's content at one year is due to partial carbonation as indicated in the text.

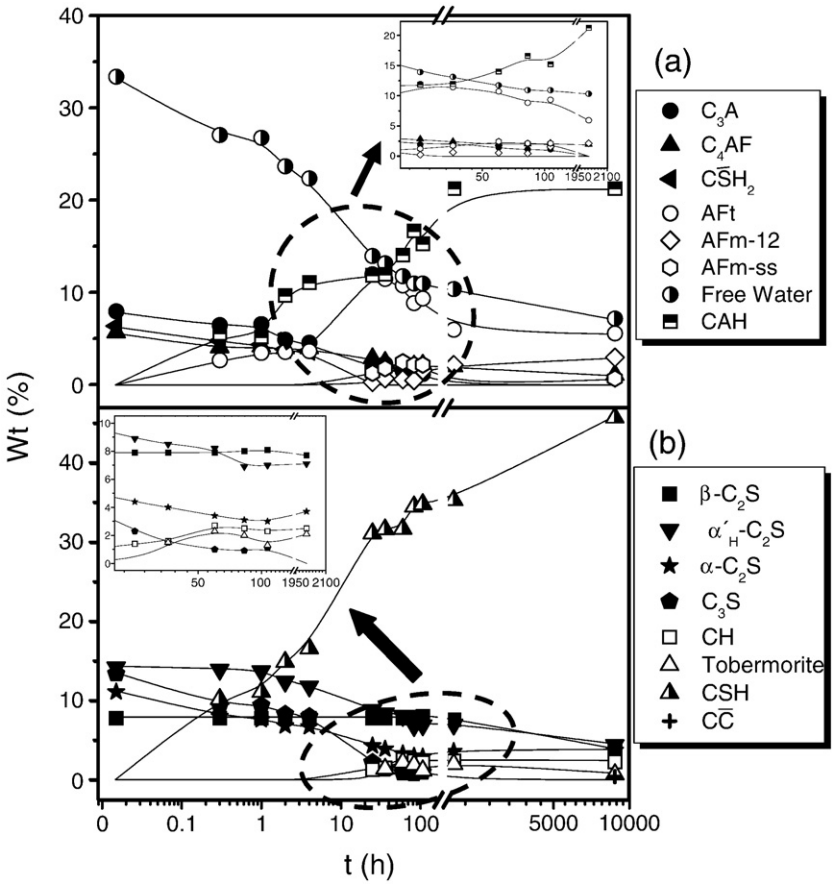

Fig. 4. Normalized quantitative Rietveld results for hydrated CB_1.5Na up to 8760 h, i.e. one year. (a) non-silicate type phases reactions and (b) silicate reactions.

of hydration and always $x<y$. Normalized t_0 phase assemblage for all the cements are shown in Figs. 3, 4 and 5. For example, to obtain normalized QPA at $t_{0.3}$ of CB_ref, normalized QPA at t_0 (the previous time) is used. Thus, normalized phase assemblage at t_0 is: 29.4 wt.% of β-C_2S, 11.7 wt.% of α_H'-C_2S, 8.3 wt.% of C_3S, 6.3 wt.% of C_3A, 7.2 wt.% of C_4AF, 3.7 wt.% of gypsum and 33.3 wt.% of free water. On the other hand, $t_{0.3}$ direct Rietveld results are given in Table 3. Analysing the data, it can be concluded that only ettringite (AFt) is appearing according to the following reaction (1):

$$C_3A + 3C\bar{S}H_2 + 26H \rightarrow C_6A\bar{S}_3H_{32}. \quad (1)$$

Thus, the amount of C_3A reacting has to be calculated as followed:

$$\frac{\beta - C_2S(t_{0.3})_R}{C_3A(t_{0.3})_R} = \frac{\beta - C_2S(t_0)_N}{C_3A(t_0)_{N-x}}$$

where β-$C_2S(t_{0.3})_R$ and $C_3A(t_{0.3})_R$ stand for Rietveld percentages of these phases at 0.3 h (Table 3), and β-$C_2S(t_0)_N$ and $C_3A(t_0)_N$ stand for percentages of these phases at normalized t_0, and x is the amount of C_3A reacting according to Eq. (1). In this example, $x=1.9$, thus the amount of water reacting is 3.5 wt.%. Finally to normalize $t_{0.3}$, direct Rietveld results are recalculated to include 29.8 wt.% of free water. This strategy has to be followed to normalize each Rietveld QPA results, for the three cements up to t_{8760}. During the first hours, i.e. the induction period, the main reaction is the formation of AFt.

The reactivity of C_4AF, to form AFt phases, has been described [47] as follows(Eq. (2)):

$$C_4AF + 4C\bar{S}H_2 + \frac{106}{3}H \rightarrow \frac{4}{3}C_6(A_{0.75}F_{0.25})\bar{S}_3H_{32} + \frac{2}{3}FH_3. \quad (2)$$

Although crystalline FH_3 has not been identified by SXRPD, and it is not possible to determine if AFt phase contains iron, the reactivity of C_4AF has also been inspected by the same strategy. The amount of C_4AF reacting at these times of hydration is negligible.

Figs. 3a, 4a and 5a show mineralogical evolution of phases involved in reaction (1) as a function of time for CB_ref, CB_1.5Na and CB_1S1NK, respectively. The behaviour of AFt (open circle) at later ages will be discussed later. Fig. 6 shows the Rietveld plot of CB_ref at $t_{2.3}$, as an example of cement paste hydrated at early ages. Main diffraction peaks of AFt, gypsum, C_4AF, C_3A, α_H'-C_2S and β-C_2S are indicated.

After some hours of hydration, the acceleration period starts and silicates begin to react [22], mainly C_3S (Eq. (3)). The α-forms of C_2S react with water (Eq. (4)) slower than C_3S.

$$C_3S + 5.3H \rightarrow C_{1.7}SH_4 + 1.3CH \quad (3)$$

$$C_2S + 4.3H \rightarrow C_{1.7}SH_4 + 0.3CH \quad (4)$$

Reactions (3) and (4) give $C_{1.7}SH_4$, which is an amorphous gel, also called C–S–H gel. The average composition, $C_{1.7}SH_4$, has been taken from [21], and it has been used to quantify the amorphous C–S–H gel

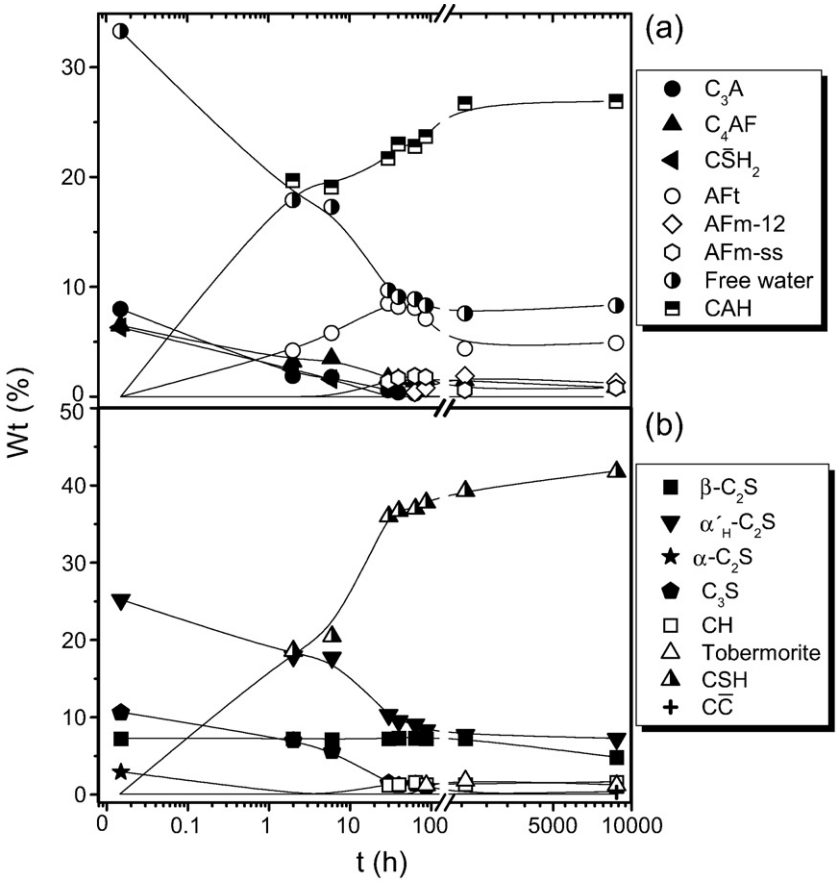

Fig. 5. Normalized quantitative Rietveld results for hydrated CB_1S1NK up to 8760 h, i.e. one year. (a) non-silicate type phases reactions and (b) silicate reactions.

that is appearing, and the diminution of water due to silicate hydration. Anhydrous C_3S is present up to t_{90}, t_{107} and t_{87} in CB_ref, CB_1.5Na and CB_1S1NK, respectively. To perform normalization, the same strategy describe above has been used. Figs. 3b, 4b and 5b show the evolution of silicate phases according to Eqs. (3) and (4).

In the acceleration period other reactions are taking place. The formation of $[Ca_2Al(OH)_6]_2SO_4\cdot 6(H_2O)$ or $C_4A\bar{S}H_{12}$ or AFm-12 phase, from C_3A and AFt, is given in reaction (5):

$$2C_3A + C_6A\bar{S}_3H_{32} + 4H \rightarrow 3C_4A\bar{S}H_{12} \quad (5)$$

Kuzel [48] found an isostructural AFm-12 containing Fe^{3+}. Recently, Meller et al. [49] have studied the C_4AF hydration with and without gypsum. They described, that at certain experimental conditions not only iron-AFt was formed but also an iron-AFm-type phase. Related to this iron-AFm-12 phase, the following reaction (6) is also assumed to take place:

$$1.5C_4AF + C_6A\bar{S}_3H_{32} + 7H \rightarrow 3C_4A_{0.5}F_{0.5}\bar{S}H_{12} + AH_3 \quad (6)$$

The formation of AFm-12 has been confirmed in the three compositions studied. This phase has been quantified using the reported structural description [44]. We have used the crystalline phase ratios, similar to that expressed above, to elucidate the reactivity of C_3A and C_4AF to form AFm-12, according to Eqs. (5) and (6). However, XRD patterns of AFm-12 and iron-AFm-12 are almost coincident, so it is only considered a global percentage of AFm-12. Reactions (5) and (6) are significant if the amount of gypsum is not optimum. The formation of AFm phases may play a non-negligible effect in the lost of plasticity in the cement paste. In the absence of calcium sulphates, AFm-type phases are formed which cause a quick set also known as "flash set" of the paste, associated with an intensive liberation of heat. Moreover, mechanical strengths developed by such pastes are usually reduced, probably due to a weakening of the microstructure by the formation of these phases [50]. CB_ref contains less gypsum than active belite cements, so reactivity of remaining C_3A and C_4AF with AFt and/or CH to form AFm-type phases is more complex. Fig. 7 shows the low angle region of the Rietveld plot of SXRPD pattern for CB_ref at t_{67}. Main peaks in this region have been labelled. Different basal *d*-spacings have been measured at this region: 10.4, 9.5, 8.9 and 8.4 Å. They have been assigned to AFm-type phases: C_2AH_8, AFm-14, AFm-12 and AFm-ss, respectively. It is well known that C_2AH_8 is an AFm-type phase with an interplanar space closed to 10.7 Å [24]. It has been described that AFm-14 [$C_4A\bar{S}H_{14}$] has the interlayer spacing at 9.5 Å [22]. On the other hand, AFm-type phases are layered structures with anions in the interlayer spaces. In AFm-12 or AFm-14, SO_4^{2-} anions are located in the interlayer space, and they can be partial or totally replaced by other anions. In these experimental conditions, it has been considered that 8.4 Å *d*-spacing value corresponds to an AFm-type, where half of the sulphate anions are replaced by OH^-, i.e. $[Ca_2Al(OH)_6]_2[SO_4,OH]\cdot 6(H_2O)$, and hereafter called as AFm-ss [51]. In order to justify the presence of these phases the following reactions (7–9) have been considered:

$$2C_3A + 27H \rightarrow C_2AH_8 + C_4AH_{19} \quad (7)$$

$$2C_3A + C_6A\bar{S}_3H_{32} + 10H \rightarrow 3AFm - 14 \quad (8)$$

$$C_3A + CH + AFm - 12 + 12H \rightarrow AFm - ss \quad (9)$$

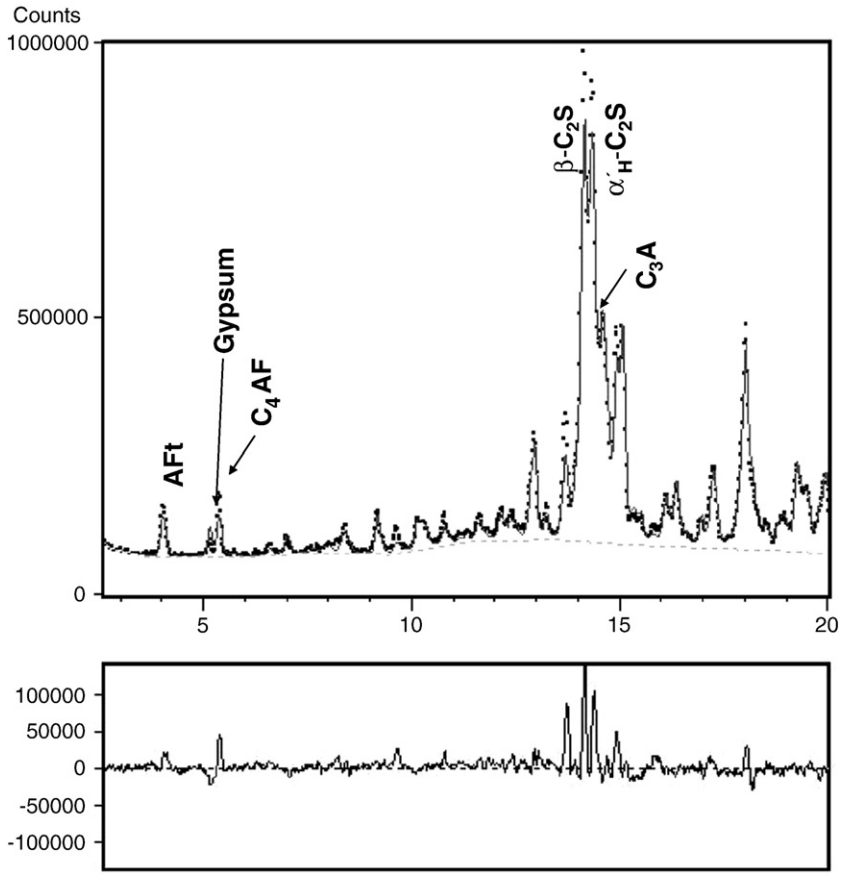

Fig. 6. Rietveld plot for CB_ref at $t_{2.3}$ showing the experimental data as points, the calculated pattern as a solid line, and the difference curve at the bottom. Main peaks for key phases have been labeled.

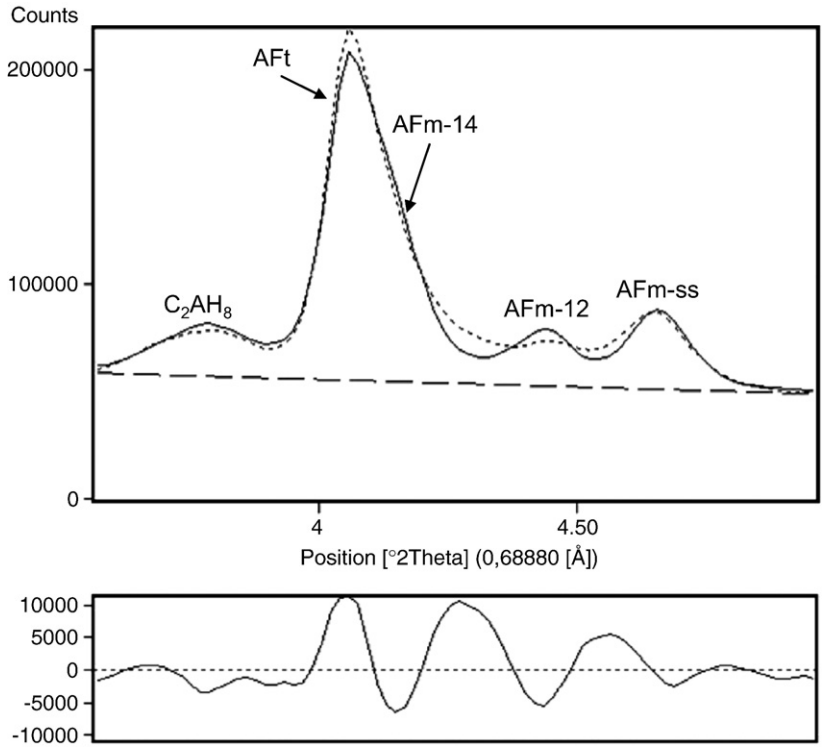

Fig. 7. Low angle detail of the Rietveld plot for CB_ref at t_{67}. Points are the experimental scan, solid line is the calculated pattern and the difference curve is given at the bottom. Main peaks for AFt and AFm-type phases are labeled.

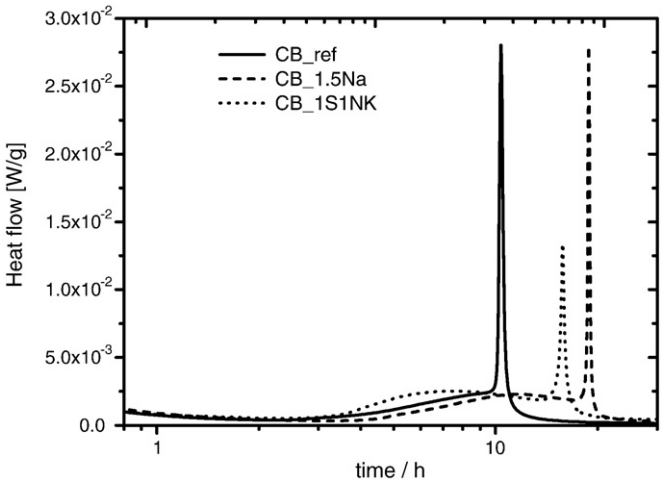

Fig. 8. Calorimetric heat flow curves for the three cements in the 0–30 h interval.

The crystal structure published in [44] for AFm-12 has been used to fit AFm-14 and AFm-ss adjusting the *c*-values. Although C_2AH_8 is also an AFm-type phase, there is not a full structural description published for this phase. So, to analyse this phase in CB_ref, we have used an average hexagonal structural model, s. g. $P6_122$, with $a = b = 5.7880$ Å and $c = 64.5018$ Å, obtained by SXRPD *ab initio* structure determination, and to be reported elsewhere. We have to highlight that two phases are formed in reaction (7), C_2AH_8 and C_4AH_{19}. X-ray patterns of these two phases are very similar, so we have quantified both as one phase, with C_2AH_8 stoichiometry.

To conclude the normalization, it has to be borne in mind that the determined fractions of AFm-type crystalline phases are smaller than those derived from the consumption of C_3A or C_4AF. Therefore, amorphous calcium aluminium hydrates, C–A–H gel, has to be indirectly derived [52]. At later ages, a bad crystallized C–S–H phase (indexed by $Ca_{1.5}SiO_{3.5}\cdot xH_2O$; PDF-33-0306) is observed. Calcium silicate hydrates, C–S–H gel, can be considered to be a highly dispersed precipitate of colloidal semicrystalline C–S–H phases [53]. All published structural models assume that C–S–H gel is a component of the solid solution formed by tobermorite ($Ca_5[H_2Si_6O_{18}]\cdot 8H_2O$) and jennite ($Ca_9[H_2Si_6O_{18}](OH)_8\cdot 6H_2O$) end members, or by tobermorite and Portlandite end members. This ill-crystalline phase has been quantified with the structural description published in [45]. Figs. 3b, 4b, and 5b show the evolution of the hydration of silicate phases with time. It has to be mentioned that some carbonation process has occurred after one year of hydration due to unavoidable deterioration of the Kapton slices. We have not taken into account that CO_2 is being included in the irradiated mass to perform the normalization.

The formation of the above mentioned AFm-type phases has been also confirmed by calorimetric studies. Fig. 8 shows a selected range (0–30 h) of the calorimetric curves for the three studied cements. Signal for the first 45 min of hydration has not been recorded due to experimental requirements for stabilization. The exotherms corresponding to Aft formation cannot be observed because they appear during the first 45 min. Initially, the induction period is observed, where small amount of heat is released out. This period finishes between 2 and 3 h, and the acceleration period starts. The most conspicuous effect is a sharp signal which is observed for all cements in the interval 10 to 20 h of hydration. These signals are due to the formation of AFm phases and the process occurs earlier in CB_ref than in the remaining cements because this cement contains less gypsum than the others. Overall heat evolved for 6 days were: 185.4, 240.5 and 194 J/g, corresponding to CB-ref, CB_1.5Na and CB_1S1NK, respectively. It can be observed that active belite cements develop higher heat than CB_ref.

After the quantitative phase analysis and the renormalization step, the degree of reaction of each phase can be calculated at a given time according to Eq. (10). In addition, the role of alkaline oxide activation of belite clinkers in the hydration processes can be properly followed. Table 6 lists the degree of reaction for all clinker phases at early (~1 and ~4 days), and later (~3 months and 1 year) ages. Several conclusions can be drawn by inspecting Table 6: i) α-C_2S phase, stabilized at room temperature by the alkaline oxide activation, hydrates slightly faster than α_H'-C_2S, however 1/3 remains unhydrated in CB_1.5Na after one year; ii) α_H'-C_2S reacts with water at a slow pace in common belite cement and somewhat faster in active belite cements, but only between half to two-thirds hydrate during the first three months; iii) β-C_2S does not hydrate during the first three months in any cement; iv) β-C_2S degree of reaction after one year is higher in belite cements activated with alkaline/sulphur oxide than in common one; v) C_3A and C_3S are the phases with larger degree of reaction at a given time, as expected; vi) the degree of reaction of C_4AF varies enormously depending upon the sulphate content and the pH of the pastes. The C_4AF reaction degree after 3 months ranges from 40% for CB_ref, which had lower gypsum content and lower amount of Portlandite, to 80% for CB_1S1NK, which had larger gypsum addition.

$$\textit{Degree of reaction of phase} - n(\%) = \frac{W^{t_0}_{\text{phase}-n} - W^{t}_{\text{phase}-n}}{W^{t_0}_{\text{phase}-n}} \times 100 \quad (10)$$

Finally, it must be noted that is not possible to properly calculate the errors associated to the reported phase assemblages for the pastes. This is so because the approximations that are needed in order to apply this methodology. Some weaknesses are pointed out: i) the compositions of some phases are variable (the clearest case, but not the only one, is gel CSH in Eqs. (3) and (4)); ii) the crystal structures of some phases are not fully known, iii) fitting the background of a pattern for a paste is not trivial; and iv) sometimes there are several competing reactions that make take place. However, this methodology allows obtaining quantitative phases analyses of pastes which are useful for a number of applications including the comparison of the hydration behaviours between active and standard belite cements.

4. Conclusions

A methodology to analyse the phase evolution of cement pastes is developed. QPA of synchrotron diffraction data for high belite cements allows establishing that β-C_2S almost does not react during the first three months. High-temperature C_2S polymorphs (α_H' and α) react faster, but

Table 6
Degree of reaction (%) for clinker phases in the cement pastes at three selected times: ~1 day, ~4 days, 3 months and 1 year.

Phase	CB_ref				CB_1.5Na				CB_1S1NK			
	23 h	114 h	3 months	1 year	25 h	107 h	3 months	1 year	30 h	87 h	3 months	1 year
β-C_2S	0	0	~0	14	0	0	~0	51	0	0	~0	33
α_H'-C_2S	19	44	44	58	38	50	50	69	59	67	69	69
α-C_2S	–	–	–	–	61	67	67	67	100	100	100	100
C_3S	39	100	100	100	83	93	100	100	86	91	100	100
C_3A	100	100	100	100	76	86	100	100	93	100	100	100
C_4AF	14	35	39	39	50	64	65	82	74	78	78	86

after one year there is still between 29 and 42% unreacted α_H'-C_2S. The hydration behaviour of different phases and polymorphs has been determined including the degree of reaction of all clinker phases. Activation with alkaline oxides increases only moderately the hydration rate of belite phases.

Acknowledgments

We thank financial support from P06-FQM-01348 research grant (Junta de Andalucía, Spain). ESRF is thanked for the provision of X-ray synchrotron powder diffraction beam time.

References

[1] J.S. Damtoft, J. Lukasik, D. Herfort, D. Sorrentino, E.M. Gartner, Sustainable development and climate change initiatives, Cem. Concr. Res. 38 (2) (2008) 115–127.
[2] A.K. Chatterjee, High belite cements. present status and future technological options: part I and part II, Cem. Concr. Res. 26 (8) (1996) 1213–1237.
[3] P.K. Mehta, Investigation on energy-saving cements, World Cem. Technol. 11 (5) (1980) 166–177.
[4] A.G. De la Torre, M.A.G. Aranda, A.H. De Aza, P. Pena, S. De Aza, Belite portland clinkers. Synthesis and mineralogical analysis, Bol. Soc. Esp. Ceram. V 44 (3) (2005) 185–191.
[5] C.D. Popescu, M. Muntean, J.H. Sharp, Industrial trial production of low energy belite cement, Cem. Concr. Composites 25 (7) (2003) 689–693.
[6] A. Gies, D. Knofel, Influence of alkalies on the composition of belite-rich cement clinkers and the technological properties of the resulting cements, Cem. Concr. Res. 16 (3) (1986) 411–422.
[7] G.S. Li, E.M. Gartner, High-belite sulfoaluminate clinker: fabrication process and binder preparation, French patent application 04-51586 (publication 2873366), 27/01/2006.
[8] K. Morsli, A.G. De la Torre, M. Zahir, M.A.G. Aranda, Mineralogical phase analysis of alkali and sulfate bearing belite rich laboratory clinkers, Cem. Concr. Res. 37 (2007) 639–646.
[9] K. Morsli, A.G. De la Torre, S. Stöber, A.J.M. Cuberos, M. Zahir, M.A.G. Aranda, Quantitative phase analysis of laboratory active belite clinkers by synchrotron powder diffraction, J. Am. Ceram. Soc. 90 (10) (2007) 3205–3212.
[10] S.N. Ghosh, P.B. Rao, A.K. Paul, K. Raina, Review. The chemistry of dicalcium silicate mineral, J. Mater. Sci. 14 (1979) 1554–1566.
[11] I. Jelenic, A. Bezjak, M. Bujan, Hydration of B_2O_3-stabilized α′- and β-modifications of dicalcium silicate, Cem. Concr. Res. 8 (2) (1978) 173–180.
[12] J. Bensted, Some hydration studies of α-dicalcium silicate, Cem. Concr. Res. 9 (1) (1979) 973-102.
[13] A.G. De la Torre, K. Morsli, M. Zahir, M.A.G. Aranda, In situ synchrotron powder diffraction study of active belite clinkers, J. Appl. Crystallog. 40 (2007) 999–1007.
[14] H.M. Rietveld, A profile refinement method for nuclear and magnetic structures, J. Appl. Crystallogr. 2 (2) (1969) 65–71.
[15] A.G. De la Torre, A. Cabeza, A. Calvente, S. Bruque, M.A.G. Aranda, Full phase analysis of Portland clinker by penetrating synchrotron powder diffraction, Anal. Chem. 73 (2001) 151–156.
[16] N.V.Y. Scarlett, I.C. Madsen, C. Manias, D. Retallack, On-line X-ray diffraction for quantitative phase analysis: application in the Portland cement industry, Powder Diffr. 16 (2) (2001) 71–80.
[17] A.G. De la Torre, M.A.G. Aranda, Accuracy in Rietveld quantitative phase analysis of Portland cements, J. Appl. Crystallogr. 36 (5) (2003) 1169–1176.
[18] V.K. Peterson, A.S. Ray, B.A. Hunter, A comparative study of Rietveld phase analysis of cement clinker using neutron, laboratory X-ray, and synchrotron data, Powder Diffr. 21 (1) (2006) 12–18.
[19] A.G. De la Torre, S. Bruque, M.A.G. Aranda, Rietveld quantitative amorphous content analysis, J. Appl. Crystallogr. 34 (2001) 196–202.
[20] P.M. Suherman, A.V. Riessen, B. O'connor, D. Li, D. Bolton, H. Fairhurst, Determination of amorphous phase levels in Portland cement clinker, Powder Diffr. 17 (3) (2002) 178–185.
[21] K.L. Scrivener, T. Fullmann, E. Gallucci, G. Walenta, E. Bermejo, Quantitative study of Portland cement hydration by X-ray diffraction/Rietveld analysis and independent methods, Cem. Concr. Res. 34 (9) (2004) 1541–1547.
[22] H.F.W. Taylor, Cement Chemistry, Thomas Telford Ltd, London, 1997.
[23] A.G. De la Torre, A. Cabeza, E.R. Losilla, M.A.G. Aranda, Quantitative phase analysis of ordinary Portland cements using synchrotron radiation powder diffraction, Z. Kristallogr. 23 (2006) 587–592.
[24] E.M. Gartner, J.F. Young, D.A. Damidot, I. Jawed, Hydration of Portland cement, in: J. Bensted, P. Barnes (Eds.), Structure and Performance of Cements, Spon Spress, London and New York, 2002.
[25] L.D. Mitchell, J.C. Margeson, P.S. Whitfield, Quantitative Rietveld analysis of hydrated cementitious systems, Powder Diffr. 21 (2) (2006) 111–113.
[26] J. Neubauer, F. Goetz-Neunhoeffer, U. Holland, D. Schmitt, P. Gaeberlein, M. Degenkolb, Crystal chemistry and microstructure of hydrated phases occurring during early OPC hydration, Proceedings of the 12th International Congress of Cement Chemistry, Montreal, 2007, W1-06.3.
[27] N. Meller, C. Hall, K. Kyritsis, G. Giriat, Synthesis of cement based CaO–Al2O3–SiO2–H2O (CASH) hydroceramics at 200 and 250 C: ex-situ and in-situ diffraction, Cem. Concr. Res. 37 (6) (2007) 823–833.
[28] A.C. Jupe, X. Turrillas, P. Barnes, S.L. Colston, C. Hall, D. Häusermann, M. Hanfland, Fast in situ X-ray diffraction studies of chemical reactions: a synchrotron view of the hydration of tricalcium aluminate, Phys. Rev. B 53 (1996) R14697–R14700.
[29] M. Merlini, G. Artioli, C. Meneghini, T. Cerulli, A. Bravo, F. Cella, The early hydration and the set of Portland cements: in situ X-ray powder diffraction studies, Powder Diffr. 22 (3) (2007) 201–208.
[30] A.C. Jupe, A.P. Wilkinson, K. Luke, G.P. Funkhouser, Slurry consistency and in situ synchrotron X-ray diffraction during the early hydration of portland cements with calcium chloride, J. Am. Ceram. Soc. 90 (8) (2007) 2595–2602.
[31] S.M. Clark, P. Barnes, A comparison of laboratory, synchrotron and neutron diffraction for the real time study of cement hydration, Cem. Concr. Res. 25 (1995) 639–646.
[32] W.E. Haskell, Three factors govern optimum gypsum content of cement, rock products, April 1959, pp. 108–149.
[33] R.H. Bogue, Calculation of the compounds in Portland cement, Ind. Eng. Chem. Anal. Ed. 1 (4) (1929) 192–197.
[34] A.P. Hammersley, S.O. Svensson, M. Hanfland, A.N. Fitch, D. Häusermann, Two-dimensional detector software: from real detector to idealised image or two-theta scan, High Pressure Res. 14 (1996) 235–248.
[35] C. Meneghini, G. Artioli, A. Balerna, A.F. Gualtieri, P. Norby, Multipurpose imaging-plate camera for in-situ powder XRD at the GILDA beamline, J. Synchrotron Radiat. 8 (2001) 1162–1166.
[36] P. Thompson, D.E. Cox, J.B. Hasting, Rietveld refinement of Debye–Scherrer synchrotron X-ray data from Al_2O_3, J. Appl. Crystallogr. 20 (2) (1987) 79–83.
[37] W.G. Mumme, R.J. Hill, G. Bushnell-Wye, E.R. Segnit, Rietveld structure refinement, crystal chemistry and calculated powder diffraction data for the polymorphs of dicalcium silicate and related phases, Neues Jahrb. Mineral. Abh. 169 (1) (1995) 35–68.
[38] A.G. De la Torre, S. Bruque, J. Campo, M.A.G. Aranda, The superstructure of C_3S from synchrotron and neutron powder diffraction and its role in quantitative phase analyses, Cem. Concr. Res. 32 (9) (2002) 1347–1356.
[39] P. Mondal, J.W. Jeffery, The crystal structure of tricalcium aluminate, $Ca_3Al_2O_6$, Acta Crystallogr. B31 (1975) 689–697.
[40] A.A. Coville, S. Geller, The crystal structure of brownmillerite, Ca_2FeAlO_5, Acta Crystallogr. B27 (1971) 2311–2315.
[41] A.G. De la Torre, M.G. López-Olmo, C. Alvarez-Rua, S. García-Granda, M.A.G. Aranda, Structure and microstructure of gypsum and its relevance to Rietveld quantitative phase analyses, Powder Diffr. 19 (3) (2004) 240–246.
[42] F. Goetz-Neunhoeffer, J. Neubauer, Refined ettringite (Ca6Al2(SO4)3(OH)12 26 (H2O)) structure for quantitative X-ray diffraction analysis, Powder Diffr. 21 (1) (2006) 4–11.
[43] H.E. Petch, The hydrogen positions in portlandite, $Ca(OH)_2$, as indicated by the electron distribution, Acta Crystallogr. 14 (1961) 950–957.
[44] R. Allmann, Refinement of the hybrid layer structure $(Ca_2Al(OH)_6)^+$ $(0.5SO_4 \cdot 3H_2O$, Neues Jahrb. Mineral. Monatsh. (1977) 136–144.
[45] E. Bonaccorsi, S. Merlino, A.R. Kampf, The crystal structure of tobermorite 14 Å (plombierite), a C–S–H phase, J. Am. Ceram. Soc. 88 (3) (2005) 505–512.
[46] B. Pokroy, J.S. Fieramosca, R.B. Von Dreele, A.N. Fitch, E.N. Caspi, E. Zolotoyabko, Atomic structure of biogenic aragonite, Chem. Mater. 19 (2007) 3244–3251.
[47] M. Fukuhara, S. Goto, K. Asaga, M. Daimon, R. Kondo, Mechanisms and kinetics of C_4AF hydration with gypsum, Cem. Concr. Res. 11 (3) (1981) 407–414.
[48] H.J. Kuzel, Substitute of Al^{3+} by Cr^{3+} and Fe^{3+} in 3CaO Al_2O_3 $CaCl_2$ nH_2O and 3CaO Al_2O_3 $CaSO_4$ nH_2O, Zem Kalk Gips 21 (12) (1968) 493–499.
[49] N. Meller, C. Hall, A.C. Jupe, S.L. Colston, S.D.M. Jacques, P. Barnes, J. Phipps, The paste hydration of brownmillerite with and without gypsum: a time resolved synchrotron diffraction study at 30, 70, 100 and 150 ºC, J. Mater. Chem. 14 (2004) 428–435.
[50] I. Odler, Hydration, setting and hardening of Portland cement, Lea´s. Chemistry of cement and concrete, Fourth Edition, 1998.
[51] T. Matschei, B. Lothenbach, F.P. Glasser, The AFm phase in Portland cement, Cem. Concr. Res. 37 (2) (2007) 118–130.
[52] J. Bensted, Calcium aluminate cements, in: J. Bensted, P. Barnes (Eds.), Structure and Performance of Cements, Spon Spress, London and New York, 2002.
[53] K. Garbev, G. Beuchle, M. Bornefeld, L. Black, P. Stemmermann, Cell dimensions and composition of nanocrystalline calcium silicate hydrate solid solutions. Part 1: synchrotron-based X-ray diffraction, J. Am. Ceram. Soc. 91 (9) (2008) 3005–3014.